Journal of Alloys and Compounds 513 (2012) 300–303

Contents lists available at SciVerse ScienceDirect

Journal of Alloys and Compounds

journal homepage: www.elsevier.com/locate/jallcom

Dielectric enhancement of $BaTiO_3/SrTiO_3$ superlattices with embedded Ni nanocrystals

Zhengwei Xiong[a,b], Weiguo Sun[a], Xuemin Wang[b], Fan Jiang[a], Weidong Wu[b,*]

[a] Institute of Atomic and Molecular Physics, Sichuan University, 610064 Chengdu, China
[b] Research Center of Laser Fusion, CAEP, P.O. Box 919-983, 621900 Mianyang, China

ARTICLE INFO

Article history:
Received 15 August 2011
Received in revised form
23 September 2011
Accepted 28 September 2011
Available online 21 October 2011

Keywords:
Ferroelectrics
Reflection high-energy electron diffraction
Scanning electron microscopy

ABSTRACT

The self-organized Ni nanocrystals (NCs) were embedded in $BaTiO_3/SrTiO_3$ superlattices using laser molecular beam epitaxy (L-MBE). The stress of the composite films was increased with the increasing concentration of embedded Ni NCs, as investigation in stress calculation. The influence with the various concentrations of Ni NCs embedded in $BaTiO_3/SrTiO_3$ superlattices was also discussed. The internal stress of the films was too strong to epitaxial growth of $BaTiO_3/SrTiO_3$ superlattices. Compared with the pure $BaTiO_3/SrTiO_3$ superlattices, the $BaTiO_3/SrTiO_3$ superlattices with lower concentration of embedded Ni NCs had higher permittivity and dielectric loss. Furthermore, the dielectric enhancement of $BaTiO_3/SrTiO_3$ superlattices with embedded Ni NCs was proposed to explained by Drude quasi-free-electron theory.

1. Introduction

Ferroelectric materials have attracted an increasing attention, especially $BaTiO_3$ (BTO)/$SrTiO_3$ (STO) superlattices, as an important class of functional materials with a variety of present and potential applications as well as a fundamental interest in high dielectric constant, nonzero remnant polarization, and nonlinear dielectric properties [1–5]. Therefore, extensive research has been carried out to obtain large dielectric constant and nonlinear dielectric properties since the dielectric properties are of fundamental importance in ferroelectric thin film devices. But up to now, we note that all the previous reported BTO/STO superlattices have a limited dielectric constant. There is also a fundamental interest in the study of artificial superlattices structures of ferroelectric oxides for the ability to improve the property of materials through structure modification [6–9]. Among these ferroelectrics materials, the dielectric matrix with the embedded metal NCs shows a great potential for a variety of technological applications such as nonlinear optical and electronic device [10–12]. Wu et al. have successfully fabricated Co–BTO and Ni–BTO composite film using self-organized method [13,14]. To our knowledge, the influence with the various concentrations of metal nanocrystals embedded in BTO/STO superlattices is seldom reported.

The growth processes of BTO/STO superlattices with embedded Ni NCs (Ni–BTO/STO) have been reported by Ge et al. [15]. In the present work, the Ni–BTO/STO composite film was fabricated by L-MBE. The influence of BTO/STO superlattices with the various concentrations of embedded Ni NCs was discussed. The structure of the composite film was confirmed by X-ray diffraction (XRD) with Cu K_α radiation and high-resolution transmission electron microscopy (HRTEM) characterization. The dielectric enhancement of the film was also investigated by the dielectric spectroscopy.

2. Experimental

The composite film was grown on STO (0 0 1) substrate with BTO/STO buffer layers by L-MBE. The growth process was performed in an ultrahigh-vacuum (UHV) system and the background vacuum was $\sim 2 \times 10^{-6}$ Pa. The experimental parameters were listed in Table 1. The acceleration voltage of RHEED electron gun was 25 keV and the grazing incidence angle was 1–3°. Before the deposition, the substrate STO (0 0 1) was in situ annealed 2 h in order to remove surface contamination. During the growth processes, the embedded Ni NCs were alternated with 7 times to grow 130-nm-thick composite film. At 10 Pa oxygen pressure, the sample was annealed about 20 min after accomplishing every BTO layer.

3. Results and discussion

Fig. 1 is the cross-section HRTEM image of 1000 pulses Ni embedded in BTO/STO superlattices. The irregular interfaces of strained Ni NC layers were alternated with 7 times. We estimated that the sizes of Ni NCs were about 3–5 nm. The individual BTO layer and STO layer have the uniform thickness of 8 nm and 10 nm, respectively. The perfect layer-by-layer epitaxial growth of STO and BTO is shown. However, there are some dislocations between the different interfaces, attributed to the strain derived from embedded Ni NCs.

* Corresponding author. Tel.: +86 816 2490535; fax: +86 816 2490535.
E-mail address: wuweidongding@163.com (W. Wu).

0925-8388/$ – see front matter © 2011 Elsevier B.V. All rights reserved.
doi:10.1016/j.jallcom.2011.09.103

Table 1
The experimental parameters for the Ni–BTO/STO film fabrication.

Background vacuum	$\sim 2 \times 10^{-6}$ Pa
Working vacuum	$\sim 2 \times 10^{-5}$ Pa
Target	$BaTiO_3$ purity > 99.99%
	$SrTiO_3$ purity > 99.99%
	Ni purity > 99.99%
Substrate	$SrTiO_3$(0 0 1)
Laser pulse frequency	1 Hz for $SrTiO_3$ deposition
	1 Hz for $BaTiO_3$ deposition
	2 Hz for Ni deposition
Energy density	248 nm 3–4 J/cm^2
The distance between the target and substrate	5 cm
Annealing condition	650 °C, 20 min
	10 Pa O_2 pressure

Fig. 2 shows the X-ray diffraction θ–2θ scans of different Ni pulses embedded in the BTO/STO superlattices. Compared with the pure BTO/STO superlattices shown in Fig. 2(a), the diffraction angles for the composite film Ni–BTO/STO are shifted to some extent shown in Fig. 2(b) because of its internal stress. According to the Bragg diffraction, the stress of the films could be calculated to STO standard:

$$\sigma = A\Delta l = \frac{E}{\nu}\Delta l = \frac{E}{\nu}\frac{(d_n/(\cos(\theta_n - \alpha))) - (d_0/(\cos(\theta_0 - \alpha)))}{d_0/(\cos(\theta_0 - \alpha))} \quad (1)$$

where E and ν represent the Yang's model and Poisson's ratio of the STO substrate, The constant A equals to E/ν. α (0.5°) represents the angle of incidence, d_0 (3.905 Å) and d_n represent the interplanar distance of the STO substrate before and after the deposition, θ_0 and θ_n represent the diffraction angle of the STO substrate before and after the deposition, respectively. The surface-lattice parameter, which is proportional to the inverse of the distance between the different diffraction spots or streaks, can be directly measured from the RHEED patterns [14,16]. By measuring the diffraction streak spacing of STO shown in the insets (e), (f) and (g), the lattice constant (d_n) in cubic structure was confirmed in real space. According to the Eq. (1), the stress of the films was calculated with the criterion of STO (0 0 2) substrate (θ_0 = 46.48°), as shown in Table 2. It is obvious that the internal stress of the films was increased from 0.0074 A MPa to 0.0268 A MPa after completing 1000 pulses Ni embedded into BTO/STO superlattices.

As shown in Fig. 2(b), it is obvious that *c*-axis oriented epitaxial growth of BTO/STO superlattices with 1000 pulses Ni NCs embedded were successfully obtained. Interestingly, the (0 0 *l*) peaks of STO were shifted to smaller angles compared with the (0 0 1) and (0 0 2) diffraction peaks located at 22.54° and 46.48° for bulk STO, respectively. It indicates that the out of plane *c*-axis lattice constant of STO was enlarged. The result is attributed to the compressive stress caused by the lattice mismatch. Due to the different lattice constant for BTO/STO, Ni/BTO, STO/Ni, the stronger strain can exist in the composite film. Due to the less content of embedded Ni, there was not found the characteristic peaks of Ni. In Fig. 2(c), there was only found the weak peak of Ni (1 1 1). The crystallographic orientation with Ni (1 1 1) takes priority of the fcc metal structure. The appearance of the Ni (1 1 1) is supposed to utmost compressed plane in order to get minimum surface energy and remain metallic property, so as to give the flat surface to the vicinal separation layer. This way reduces extremely the effect of the strained distortion by the large lattice mismatch between the different interfaces.

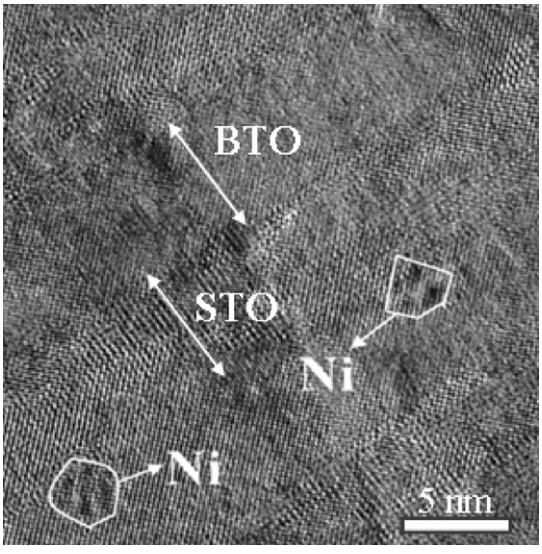

Fig. 1. The cross-section HRTEM image of 1000 pulses Ni embedded in BTO/STO superlattices.

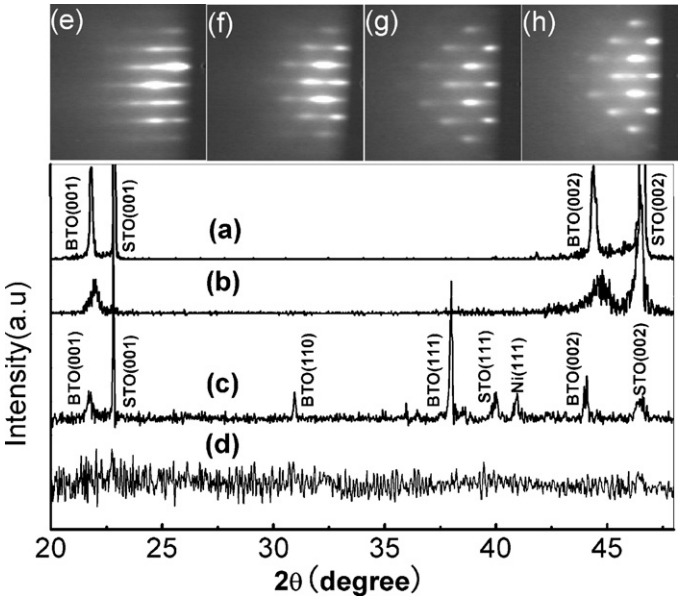

Fig. 2. XRD θ–2θ scans of the different Ni pulses embedded in the BTO/STO superlattices: (a) 0 pulse; (b) 1000 pulses; (c) 3000 pulses; (d) 5000 pulses; the corresponding diffraction RHEED patterns of STO was recorded in (e)–(h), respectively.

It is obvious that the structure of BTO/STO superlattices is transformed from polycrystal to non-crystal, while the embedded Ni pulses gradually increase, as shown in Fig. 2(a)–(d). The crystallinity of BTO and STO became worse and the epitaxial growth of BTO/STO superlattices was disturbed. In addition, the transformation of RHEED patterns from diffraction streaks to dominant spots was observed for STO layer deposited on Ni NCs shown in Fig. 2(e) and (f). The result indicates that the growth mode of STO changes from layer-by-layer mode to island mode, leading to the variation of structure. On the BTO layer at the initial stage, deposited Ni lattice is clamped in plane. Due to the large mismatch (11.2%) between BTO and Ni, strain can be partly relieved by lattice distortion with increasing the out of plane lattice constant. However, the lateral lattice constant was adjusted to the BTO lattice, result-

Table 2
The stress of the films synthesized with different pulses Ni embedded into BTO/STO superlattices.

	θ_n (°)	d_n (Å)	Stress (MPa)
Pure BTO/STO superlattices	46.54	3.93	0.0074 A
1000 pulses Ni–BTO/STO	46.46	3.97	0.0163 A
3000 pulses Ni–BTO/STO	46.34	4.02	0.0268 A

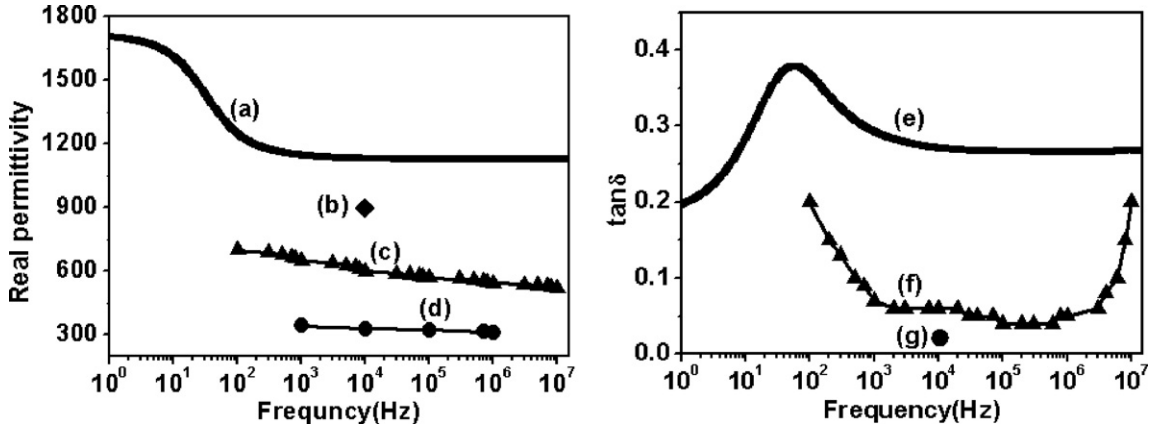

Fig. 3. (a) The variation of real permittivity (ε') with frequency at room temperature; the ε' in the insets (b)–(d) correspond to Refs. [1–3]; the inset (e) recorded the variation of dielectric loss ($\tan\delta$) with frequency at room temperature, the $\tan\delta$ in the insets (f) and (g) correspond to Refs. [2,3].

ing in lateral tensile strain and vertical compressive strain at the interface. With the increasing of Ni pulses, the concentration of Ni NCs also increases. In this irregular strained layer, the elastic strain energy increases with the concentration of Ni NCs. The strain energy becomes much larger and the internal stress cannot be fully relieved. After the initial growth of Ni, strain-island model can be explained the growth process of Ni NCs. In this way, the enlarged surface due to the formation of 3D islands can reduce the strain energy. Moreover, the film lattices are misoriented with each other, resulting in a polydomain structure at this stage shown in Fig. 2(c). But if the strained islands combined with polydomain structure are no longer sufficient to relieve stress during the deposition process, stress relief will begin to smooth the surface by introducing misfit dislocations at the interface. As more Ni adatoms are deposited onto the BTO surface, the islands can combine with each other to lower the surface energy instead of giving rise to a rough layer until the complete strain relaxation state. Thus the Ni NCs is successfully embedded in BTO/STO superlattices and cannot disturb the epitaxial growth of BTO and STO. However, the excessive strain energy can disturb the epitaxial growth of BTO and STO when the large numbers of Ni adatoms are deposited onto the BTO surface. Furthermore, the worse crystallinity of composite film is presented, as shown in Fig. 2(d). This mechanism can offer a valuable approach for synthesizing quantum dots or other nanostructures. These experimental results have also been reported in Ref. [17], in which the lattice mismatch is very close to our model. Thus, it is concluded that the composite film structure of Ni–BTO/STO is changed by internal stress with the increasing concentration of Ni NCs.

Fig. 3(a) shows the variation of real permittivity (ε') with frequency at room temperature for the Ni–BTO/STO composite film with lower concentration of embedded Ni NCs. Recently, a dielectric constant of approximately 900 at 10 kHz was reported in BTO/STO superlattices with 10 stacking periodicities, as shown in Fig. 3(b). And it was found that the dielectric constant tended to decrease with the increasing stacking periodicity [1]. Compared with published literature about BTO/STO superlattices shown in Fig. 3(b)–(d) [1–3], the value of ε' for BTO/STO superlattices with embedded Ni NCs was enhanced. According to Drude quasi-free-electron theory, the relative permittivity of metal are given by

$$\varepsilon(\omega) = 1 - \frac{Ne^2}{m(\omega^2 + i\omega\gamma_0)} \tag{2}$$

here, e is the electron charge, m is electron mass. Furthermore, on the assumption that N_a electrons per unit volume begin to transition, the real and imaginary permittivity are given by

$$\varepsilon'(\omega) = 1 - \frac{Ne^2}{m}\cdot\frac{1}{\omega^2+\gamma_0^2} + \sum_a \frac{N_a e^2}{m}\cdot\frac{\omega_a^2-\omega^2}{(\omega_a^2-\omega^2)^2+\omega^2\gamma_a^2} \tag{3}$$

$$\varepsilon''(\omega) = \frac{Ne^2}{m}\cdot\frac{\gamma_0}{\omega^3+\omega\gamma_0^2} + \sum_a \frac{N_a e}{m}\cdot\frac{\omega\gamma_a}{(\omega_a^2-\omega^2)+\omega^2\gamma^2} \tag{4}$$

here, ω_a is transition frequency, γ_a is damping constant per unit mass. When the size of a metal particle ($d_{\mathrm{Ni\ Nc}} \le 5$ nm) closes to nano-grade, the Ni NC can be regarded as a small nano-globule. When electromagnetic wave [$E(t) = E_0 e^{i\omega t} + c\cdot c$] radiates the Ni NCs, the effective electric region field of metal nano-globule occurs to change. Considering the BTO/STO superlattices as uniform dielectrics (ε_m), the intensity of polarization for n nano-globules per unit volume can be shown by

$$P = \frac{n\alpha(\omega)\varepsilon_0\varepsilon_m}{1-(1/3)n\alpha(\omega)}E \tag{5}$$

where $\alpha(\omega)$ is the polarizability of metal nano-globule. It is obvious that the polarization of the composite film is enhanced by the embedded Ni NCs. The increase of dielectric constant can be attributed to the enhancement of polarization.

Fig. 3(e) shows the variation of dielectric loss ($\tan\delta$) with frequency at room temperature. Compared with the former reports for BTO/STO superlattices shown in Fig. 3(f) and (g), the higher dielectric loss is observed. It is well known that the dielectric loss of the materials reflects electromagnetic waves absorption which can be expressed by imaginary polarizability $Im\,\alpha(\omega)$ [18]. The result indicates that the absorption is enhanced. When the radius (R) of metal NCs is less than electron mean free path, accorded with our experiment, the damping constant (γ) depends on the nano-globule radius. Introducing the γ given by

$$\gamma = \gamma_0 + (A_1 + iA_2)\frac{\nu_F}{R} \tag{6}$$

here, the γ_0 is damping constant for bulk metal, ν_F is electron fermi velocity, the imaginary $\alpha(\omega)$ is deduced by

$$Im\,\alpha(\omega) = \frac{4\pi R^3\times 3\varepsilon_m\, Im\,\chi^{ib}}{M^2+(Im\,\chi^{ib})^2} + \frac{4\pi R^3\times 3\varepsilon_m\Omega^2[M\omega\, Re\,\gamma - K\, Im\,\chi^{ib}]}{[MK+\omega\, Im\,\chi^{ib}\cdot Re\,\gamma]^2+[M\omega\, Re\,\gamma - K\, Im\,\chi^{ib}]^2} \tag{7}$$

$$\Omega = \frac{\omega_p}{\sqrt{1 + 2\varepsilon_m + \chi^{ib}}} \tag{8}$$

$$M = 1 + 2\varepsilon_m + Re\,\chi^{ib} \tag{9}$$

$$K = \Omega^2 - \omega^2 + \omega\, Im\,\gamma \tag{10}$$

$$Re\,\gamma = \gamma_0 + A_1 \frac{\nu_F}{R} \tag{11}$$

$$Im\gamma = A_2 \frac{\nu_F}{R} \tag{12}$$

where Ω is the resonance frequency of metal nano-globule, χ^{ib} is independent quantity to radius of nano-globule. Thus, it is demonstrated that the higher dielectric loss derives from the increasing of resonance absorption shown by A_1.

4. Conclusion

In summary, the $BaTiO_3/SrTiO_3$ superlattices with embedded Ni NCs were fabricated by L-MBE. With the different concentrations of Ni NCs, the structure of the composite film set in transformation from polycrystal to non-crystal, attributed to the increasing internal stress. The stress of films was increased as investigation of stress calculation. In combination with published literature for pure BTO/STO superlattices, the composite film synthesized with lower concentration of Ni NCs had higher permittivity and dielectric loss. Using Drude quasi-free-electron theory, the dielectric enhancement of the films was explained. These results provided a theoretical basis for the revealing and the application developing of the characters of metal nano-materials.

References

[1] H. Tabata, H. Tanaka, T. Kawai, Appl. Phys. Lett. 65 (1994) 1970–1973.
[2] F.M. Pontes, E.R. Leite, E.J.H. Lee, E. Longo, J.A. Varela, Thin Solid Films 385 (2001) 260–265.
[3] H.N. Tsai, Y.C. Liang, H.Y. Lee, J. Crystal Growth 284 (2005) 65–72.
[4] H.N. Lee, H.M. Christen, M.F. Chisholm, C.M. Rouleau, D.H. Lownders, Nature 433 (2005) 395–399.
[5] O. Nakagawara, T. Shimuta, T. Makino, S. Arai, H. Tabata, T. Kawai, Appl. Phys. Lett. 77 (2000) 3257–3260.
[6] J.C. Jiang, X.Q. Pan, W. Tian, C.D. Theis, D.G. Schlom, Appl. Phys. Lett. 74 (1999) 2851–2853.
[7] H. Tabata, H. Tanaka, T. Kawai, M. Okuyama, Jpn. J. Appl. Phys. 34 (Part 1) (1995) 544–547.
[8] T. Tsurumi, T. Ichikawa, T. Harigai, H. Kakemoto, S. Wada, J. Appl. Phys. 91 (2002) 2284–2289.
[9] J. Kim, Y. Kim, Y.S. Kim, J. Lee, L. Kim, D. Jung, Appl. Phys. Lett. 80 (2002) 3581–3583.
[10] A. Nahata, R.A. Linke, T. Ishi, K. Ohashi, Opt. Lett. 28 (2003) 423–425.
[11] T. Shimuta, O. Nakagawara, T. Makino, S. Arai, J. Appl. Phys. 91 (2002) 2290–2294.
[12] T. Kuroiwa, Y. Tsunemine, T. Horikawa, T. Makita, J. Tanimura, N. Mikami, K. Sato, Jpn. J. Appl. Phys. 33 (1994) 5187–5191.
[13] W.D. Wu, Y.J. He, F. Wang, Z.H. Chen, Y.J. Tang, W.G. Sun, J. Crystal Growth 289 (2006) 408–413.
[14] F.F. Ge, X.M. Wang, L.H. Cao, J. Li, H.L. Zhang, H.P. Wang, Y. Dai, H.B. Wang, J. Shen, W.D. Wu, Nano Res. Lett. 5 (2010) 834–838.
[15] F.F. Ge, X.M. Wang, Y.N. Li, L.H. Cao, H.L. Zhang, H.B. Wang, W.D. Wu, J. Nanopart. Res. doi:10.1007/s11051-011-0475-z.
[16] K. Godo, J.H. Chang, H. Makino, T. Takai, T. Hanada, T. Yao, T. Sascao, T. Goto, J. Appl. Phys. 92 (2002) 5490–5493.
[17] I. Lyubinetsky, S. Thevuthasan, D.E. McCready, D.R. Baer, J. Appl. Phys. 94 (2003) 7926–7928.
[18] Ž. Crljen, D.C. Langreth, Phys. Rev. B 35 (1987) 4224–4231.